

Hyo-Sung Kwak  
Jeong-Min Lee  
Young-Kon Kim  
Young Hwan Lee  
Chong-Soo Kim

## Detection of hepatocellular carcinoma: comparison of ferumoxides-enhanced and gadolinium-enhanced dynamic three-dimensional volume interpolated breath-hold MR imaging

Received: 11 July 2004  
Revised: 22 August 2004  
Accepted: 24 August 2004  
Published online: 22 September 2004  
© Springer-Verlag 2004

H.-S. Kwak · Y.-K. Kim · C.-S. Kim  
Department of Diagnostic Radiology,  
Chonbuk National University Medical  
School,  
Chon-ju, South Korea

J.-M. Lee (✉)  
Department of Radiology,  
Seoul National University Hospital,  
28, Yongon-Dong, Chongno-Gu,  
Seoul, 110-744, South Korea  
e-mail: leejm@radcom.snu.ac.kr  
Tel.: +82-2-7603154  
Fax: +82-2-7436385

Y. H. Lee  
Department of Diagnostic Radiology,  
Wonkwang University School of Medicine,  
Iksan, South Korea

**Abstract** The purpose was to compare the diagnostic accuracy of ferumoxides-enhanced MR imaging and gadolinium-enhanced dynamic MR imaging using three-dimensional (3D) volume interpolated breath-hold examination (VIBE) for the detection of hepatocellular carcinoma (HCC). Forty-nine patients with 61 HCCs, who underwent ferumoxides-enhanced and gadolinium-enhanced dynamic MR imaging, were included prospectively in this study. Ferumoxides-enhanced MR imaging was performed 24 h after completion of the dynamic study using 3D-VIBE. Three radiologists independently interpreted the images. The diagnostic accuracy was evaluated using the receiver-operating characteristic method, and the sensitivity of each imaging technique was compared using McNemar's test. The mean diagnostic accuracy of dynamic MR

imaging ( $A_z=0.95$ ) was higher than that of ferumoxides-enhanced MR imaging ( $A_z=0.90$ ), but failed to reach a statistical significance ( $P=0.057$ ). The mean sensitivity of dynamic MR imaging (90.7%) was significantly superior to that of ferumoxides-enhanced MR imaging (80.9%,  $P=0.03$ ). Furthermore, for lesions smaller than 15 mm, the mean sensitivity of dynamic MR imaging was significantly higher than that of ferumoxides-enhanced MR imaging (85.2% vs. 69.2%,  $P<0.05$ ). Dynamic MR imaging showed a trend toward better diagnostic accuracy for than ferumoxides-enhanced MR imaging for the detection of HCCs.

**Keywords** Liver · MR imaging · Neoplasms · Magnetic resonance · Contrast agents

### Introduction

Ferumoxides-enhanced liver magnetic resonance (MR) imaging has been reported to be a very sensitive technique for the detection of focal liver malignancies, including hepatocellular carcinoma (HCC) and hepatic metastases [1–8]. Intravenously administered ferumoxides particles are ingested by macrophages of the reticulo-endothelial system, including Kupffer's cells in the liver, and predominantly increase T2 relaxation of the liver parenchyma [9]. As most malignant hepatic tumors are devoid of Kupffer's cells, except some well-differentiated HCCs, the contrast between the lesions and normal liver

tissue is remarkably improved on ferumoxides-enhanced T2-weighted MR imaging.

Because of the rapid development of MR technology, three-dimensional (3D) Fourier transformation gradient-echo (GRE) MR techniques are successfully used at many research facilities for dynamic liver MR imaging [10–12]. Recently, the volumetric interpolated breath-hold examination (VIBE), a fat-saturated 3D gradient-echo sequence with nearly isotropic resolution, has become available [13]. Using the VIBE technique, it is possible to acquire thinner sections than those previously used in the 2D GRE technique for body MR and therefore the evaluation of very small masses is feasible.

To our knowledge, a study comparing ferumoxides-enhanced MR imaging and gadolinium-enhanced dynamic 3D-VIBE MR imaging for the detection of HCC has not been performed yet. The purpose of our study is to compare the diagnostic accuracy of these two types of MR imaging for the detection of HCC.

## Materials and methods

### Patients

Between June 2002 and October 2003, 53 consecutive patients with suspected HCC on the basis of the results of previous helical CT ( $n=31$ ) or helical CT and sonography ( $n=22$ ) underwent ferumoxides-enhanced MR imaging and gadolinium-enhanced 3D-VIBE MR imaging in order to determine the ultimate therapeutic method. Four patients who underwent transcatheter arterial chemoembolization (TACE) were excluded from this study because the 6-month follow-up examinations were not performed. The remaining 49 patients were included in the study (men, 39; women, 10; age range, 47–69 years; mean age, 57 years). The institutional review board of our hospital approved this study, and written informed consent was obtained from all patients. The severity of the patients' liver cirrhosis was evaluated according to the Child-Pugh classification [14]. Thirty patients were classified with a Child score A (mild liver cirrhosis), ten patients with a Child score B (moderate liver cirrhosis) and nine patients with a Child score C (severe liver cirrhosis). Also, the hepatitis B surface antigen was positive in all patients.

### Lesion confirmation

A total of 49 patients with 61 HCCs (5–40 mm, mean 16.2 mm) were enrolled in the study. Four patients had two HCCs, 4 patients had three lesions and one nodule was confirmed in each of the remaining 41 patients. Twenty-one patients with 24 lesions underwent hepatic resection and intraoperative sonography. In the 11 patients with 11 lesions, subsequent percutaneous biopsy from representative lesions confirmed the diagnosis of HCC. For the other 17 patients with 26 lesions, the presence of each malignant lesion was confirmed based on a combination of the clinical and radiological criteria, including liver cirrhosis and viral hepatitis B, characteristic angiographic findings of HCC, elevated serum alpha-fetoprotein level (over 400 ng/ml), a response to TACE and focal retention of angiographically administered iodized oil on CT scanning.

Follow-up radiological examinations, such as triphasic-helical CT ( $n=34$ ), CT during arterial portography and CT during hepatic arteriography ( $n=17$ ) and contrast-enhanced MR imaging ( $n=20$ ), were performed in all patients at least 6 months after both the ferumoxides-enhanced and the gadolinium-enhanced MR imaging. Proof of the absence of HCC nodules in hepatic segments was provided by negative findings on intraoperative sonography or by a combination of no nodular iodized oil uptake and no evidence of further nodular growth on follow-up triphasic helical CT, angiographically assisted CT and/or MR imaging.

### MR imaging examination

All MR imaging was performed on a 1.5-T super-conducting scanner (Magnetom Symphony; Siemens, Erlangen, Germany) with phased array multicoils for signal reception.

The liver was imaged in axial planes in all of the following sequences: baseline MRIs including a respiratory-triggered T2-

weighted turbo spin-echo sequence, a breath-hold T2\*-weighted fast imaging with steady-state precession (FISP) sequence and a breath-hold T1-weighted fast low-angle shot (FLASH) sequence. Respiratory-triggered T2-weighted turbo spin-echo imaging was obtained using the following parameters: a TR/TE of 3,300–5,500/85, echo train length of 5, matrix of 120×256 and a signal average of two. Breath-hold T2\*-weighted FISP imaging was obtained using the following parameters: a TR/TE of 180/12, 30° flip angle, matrix of 96×256 and a signal average of one [15, 16]. Breath-hold T1-weighted fast low-angle shot imaging was obtained using the following parameters: a TR/TE of 120/4, 70° flip angle, matrix of 120×256 and a signal average of one. For all sequences, a 6-mm slice thickness was used with a 10% intersection gap and a field of view of 35–40 cm, depending on the size of the liver.

Dynamic imaging was performed following administration of gadopentetate dimeglumine (Magnevist; Schering, Berlin, Germany). A dose of 0.1 mmol/kg gadopentetate dimeglumine was injected using an automated injector (Spectris MR; Medrad, Germany) at a flow rate of 3 ml/s followed by injection of 20 ml of normal saline at the same flow rate. The determination of scan delay for image acquisition timing was achieved using the test bolus technique in which 1 ml of gadopentetate dimeglumine was injected along with 20 ml saline flushing; the vessel of interest (abdominal aorta at the level of the celiac axis) was scanned approximately once per second. The time to peak aortic enhancement was estimated from curves for signal intensity that were generated by means of vendor-provided software (Siemens) and the optimal imaging delay (OID) to arterial phase MR imaging (i.e., the delay time from the beginning of injection to the beginning of MR imaging) was calculated for a centric  $k$ -space-encoded sequence by means of the following formula [17]:  $OID = D_{pae} + (t_{inj}/2)$ , where  $D_{pae}$  is the delay to peak aortic enhancement and  $t_{inj}$  is the time for contrast material injection. The time for the contrast material injection was calculated by dividing the volume of contrast material by the rate of injection. The breath-hold T1-weighted FLASH imaging sequence for arterial phase (20–30 s), portal phase (45–60 s) and equilibrium phase (180 s) imaging was obtained using 3D Fourier transform gradient echo imaging (VIBE; Siemens, Erlangen, Germany) using the following parameters: TR/TE of 3.4–3.8/1.4–1.8, a flip angle of 12°, bandwidth 490 Hz/Px, a matrix of 256 (read)×120 (phase)×64–72 (partition), an effective slice thickness of 2.3 mm and a field of view of 32–35 cm [14]. All images were acquired during breath-hold, and sampling was done by 70% in the Z-direction and by 70% in the phase direction using volumetric interpolation. Image reconstruction with a 6-mm thickness was performed with source images at an MR workstation.

After completion of the dynamic MR examination, ferumoxides-enhanced MR imaging was performed with an interval of 24 h. A ferumoxides solution (Feridex IV; Advanced Magnetix, Cambridge, MA) at 10  $\mu$ mol/kg diluted in 100 ml of 5% glucose solution was infused for 30 min through a 5- $\mu$ m filter. During the first 10 min, infusion was performed at a slow rate (2 ml/min). If no adverse reaction occurred, infusion was accelerated to 4 ml/min during the remaining 20 min. MR imaging was performed from 40 min to 1 h after the infusion was completed. Ferumoxides-enhanced imaging was comprised of a respiratory-triggered T2-weighted turbo spin-echo sequence, a breath-hold T2\*-weighted FISP sequence and a breath-hold T1-weighted FLASH sequence, with the same parameters as those used in baseline MRI.

### Imaging analysis

Before performing the analysis, two experienced abdominal radiologists who served as the study coordinators in the alternative-free response operative characteristic (AFROC) analysis defined the gold standard for the presence of a lesion to be analyzed with consensus decision-making. For this purpose they were given the

images from all the imaging modalities, including intraoperative sonography, angiography, angiographically assisted CT, contrast-enhanced MR images and iodinated-oil CT, as well as the operative and histologic findings. Also, after their analysis, the two abdominal radiologists defined possible causes of the false-negative and false-positive findings.

All MR images were evaluated independently by three other abdominal radiologists experienced in interpreting MRI of the liver in their daily clinical practice for at least 5 years. They knew that the patients had liver cirrhosis and were at risk for HCC, but were blinded to the results of all the other imaging findings and the readings of the other observers as well as to the final diagnoses.

Each observer analyzed two sets of images, i.e., 3D gadopentate dimeglumine-enhanced dynamic MR images (arterial, portal and equilibrium phases) and ferumoxides-enhanced MR images (T2\*-weighted and respiratory-triggered T2-weighted turbo spin-echo images). To minimize any learning bias, there was a 2-week interval between the two readings. Each observer recorded the size and location of one or more lesions, assigning to each a confidence level on a four-point scale (1 = probably not a lesion, 2 = possibly a lesion, 3 = probably a lesion and 4 = definite lesion).

Based on the reviews of the three observers, an AFROC curve analysis was performed on a tumor-by-tumor basis [18]. For each imaging set, an AFROC curve was fitted to each observer's confidence rating data using a maximum likelihood estimation program. The diagnostic accuracy of each imaging modality was determined by calculating the area (A index,  $A_z$ ) under the AFROC curve when it was plotted in the designated square. Differences between imaging modalities in terms of the mean  $A_z$  values were analyzed statistically by means of the two-tailed Student's  $t$  test for paired data. A two-tailed  $P$  value of less than 0.05 was considered significant.

The sensitivity for each observer and each modality was determined using only those lesions allocated a confidence rating of 3 or 4. The sensitivity derived from the mean of the results obtained from all the observers was also calculated. We compared the sensitivities of each imaging modality of each observer using the McNemar's test. Differences between imaging modalities in terms of the mean sensitivity were analyzed statistically by means of the two-tailed Student's  $t$  test for paired data. A two-tailed  $P$  value of less than 0.05 was considered significant. Analysis of all false-negative and false-positive (confidence levels of 3 or 4) observations was also undertaken.

To assess the interobserver variability in interpreting the images, kappa statistics were used to measure the degree of agreement among the observers. Kappa values greater than zero were considered to indicate a positive correlation. Values up to 0.4 were considered to indicate poor correlation, values of 0.41–0.75 good correlation and values greater than 0.75 excellent correlation.

## Results

### AFROC analysis

The  $A_z$  values for each observer and the mean  $A_z$  values of the two pairs of imaging modalities are shown in Table 1. For lesion detection, all three observers achieved higher diagnostic performance with gadolinium-enhanced dynamic 3D-VIBE MR images than with ferumoxides-enhanced MR images. The mean  $A_z$  value for gadolinium-enhanced 3D-VIBE MR images ( $A_z=0.95$ ) was greater than that for ferumoxides-enhanced MR images ( $A_z=0.90$ ), but failed to reach a statistical significance ( $P=0.057$ ) [(Fig. 1)].

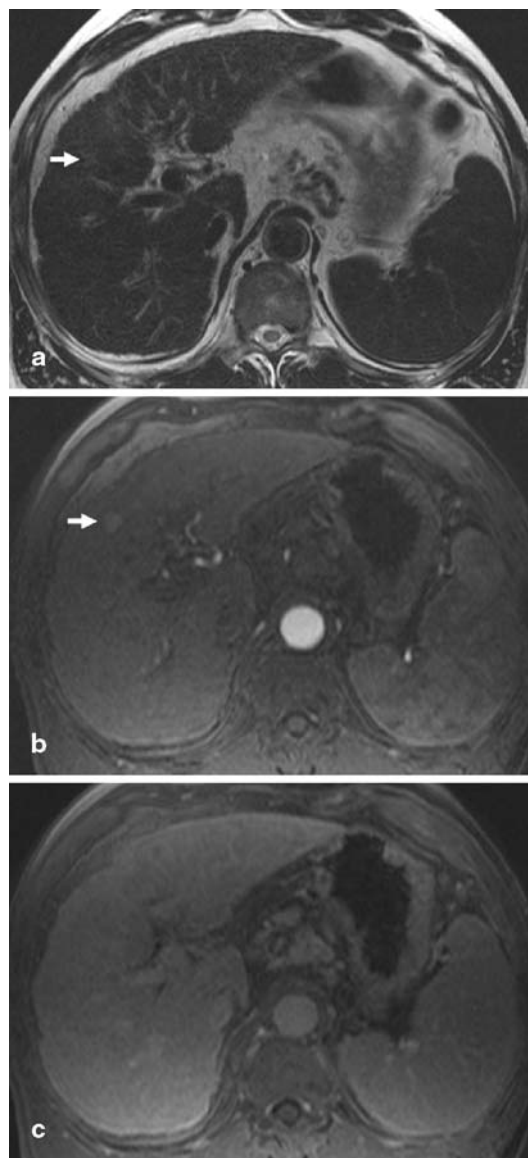


**Fig. 1** A 54-year-old man with a hepatocellular carcinoma nodule 10 mm in diameter. **a** Ferumoxides-enhanced breath-hold T2\*-weighted fast image obtained with steady-state procession shows ill-defined high-signal intensity (arrow) [(assigned a confidence level of 2 or 3)]. Note partial obscuring by adjacent liver tissue. **b** Gadolinium-enhanced 3D-VIBE image obtained during the arterial phase shows early enhancement of the small lesion (arrow) [(assigned confidence level of 5)]. **c** Equilibrium-phase MR image obtained 3 min after contrast injection demonstrates that lesions show isosignal intensity relative to surrounding liver parenchyma

### Sensitivity

The sensitivities were calculated for each observer and were also determined for each modality (Table 2). The mean sensitivity of gadolinium-enhanced dynamic 3D-VIBE MR images (90.7%) was significantly superior to that of ferumoxides-enhanced MR images (80.9%,

**Fig. 2** A 45-year-old man with a hepatocellular carcinoma 8 mm in diameter in the hepatic dome. **a** Gadolinium-enhanced 3D-VIBE image obtained during the arterial phase shows bright nodular enhancement (*arrow*). **b** The dynamic portal phase shows the isosignal intensity of nodular enhancement on the arterial phase. **c** Ferumoxides-enhanced breath-hold T2\*-weighted fat image obtained with steady-state procession shows no visible mass lesion. **d** Photograph of the surgical specimen shows tumor tissue with a trabecular pattern (H&E,  $\times 40$ )

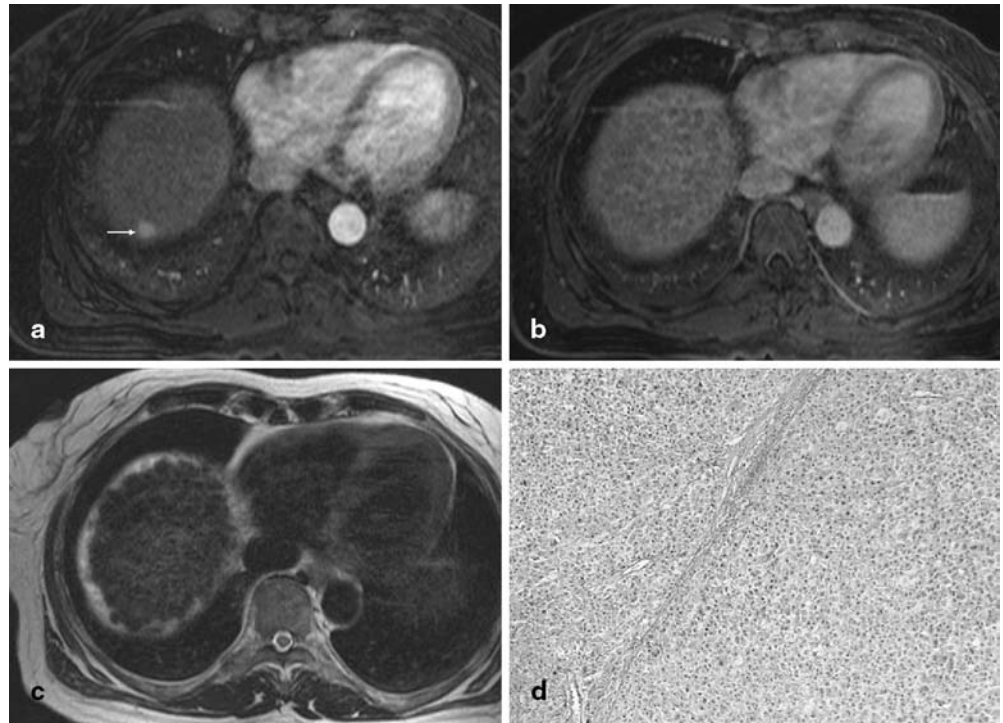


**Table 1** Az and *P* values for ferumoxides-enhanced MR imaging and gadolinium-enhanced dynamic MR imaging for the detection of hepatocellular carcinomas by three observers

Value	Observer 1	Observer 2	Observer 3	Mean
Az value				
Ferumoxides-enhanced MR imaging	0.88	0.90	0.91	0.90
Dynamic 3D-VIBE MR imaging	0.96	0.94	0.95	0.95
<i>P</i> value	0.01	0.24	0.12	0.057

VIBE volumetric interpolated breath-hold examination.

**Table 2** Individual and mean observer sensitivities for detection of hepatocellular carcinomas on ferumoxides-enhanced MR imaging and gadolinium-enhanced dynamic MR imaging by three observers

Value and imaging techniques	Number (%)		
	Observer 1	Observer 2	Observer 3
Sensitivity of 61 hepatocellular carcinomas			
Ferumoxides-enhanced MR imaging	48 (78.7)	50 (82.0)	50 (82.0)
Dynamic 3D-VIBE MR imaging	56 (91.8) <sup>a</sup>	54 (88.5)	55 (91.8)

Data represent the numbers of 61 hepatocellular carcinomas assigned a score of 3 or 4 for sensitivity.

<sup>a</sup> Sensitivity was significantly greater than that for ferumoxides-enhanced MR imaging ( $P < 0.05$ ).

$P = 0.03$ ). The detection sensitivities for HCCs of two size categories ( $\leq 15$  mm or  $> 15$  mm) for each of the three observers are shown in Table 3. The mean sensitivity of the gadolinium-enhanced dynamic 3D-VIBE MR images (85.2%) was significantly higher than that of the ferumoxides-enhanced MR images (69.4%) in lesions smaller than 15 mm ( $P < 0.05$ ) [(Fig. 2)]. The differences in the sensitivities between the two imaging modalities were not significant for any of the observers in lesions larger than 15 mm.

#### False-negative lesions

HCCs that were missed on ferumoxides-enhanced MR imaging were detected on gadolinium-enhanced dynamic 3D-VIBE MR imaging by three observers as follows: observer 1, nine tumors in eight patients; observer 2, ten tumors in nine patients; observer 3, nine tumors in eight patients. Four tumors missed by all observers on ferumoxides-enhanced MR imaging were detected on gadolinium-enhanced dynamic 3D-VIBE MR imaging

**Table 3** Sensitivity for detection of hepatocellular carcinoma by lesion size

Data represent the numbers of 61 hepatocellular carcinomas assigned a score of 3 or 4 for sensitivity.

<sup>a</sup> Sensitivity was significantly greater than that for ferumoxides-enhanced MR imaging ( $P < 0.05$ ).

Imaging type and observers	≤15 mm (n=36)	>15 mm (n=25)	Overall (n=61)
Ferumoxides-enhanced MR Imaging			
Observer 1	24 (66.7)	24 (96.0)	48 (78.7)
Observer 2	25 (69.4)	25 (100.0)	50 (82.0)
Observer 3	26 (72.2)	24 (96.0)	50 (82.0)
Dynamic 3D-VIBE MR imaging			
Observer 1	32 (88.9) <sup>a</sup>	24 (96.0)	56 (91.8)
Observer 2	30 (83.3)	24 (96.0)	54 (88.5)
Observer 3	30 (83.3)	25 (100.0)	55 (90.2)

**Table 4** Analysis of false-positive findings

Imaging technique	Ferumoxides-enhanced MR Imaging	Dynamic 3D-VIBE MR Imaging
True-positive observations	148	175
False-positive observations	25	23
False-positive rate	16.9%	13.1%

**Table 5** Agreement among observers regarding the presence of HCC

Imaging techniques	Observer 1 vs. observer 2	Observer 2 vs. observer 3	Observer 1 vs. observer 3
Ferumoxides-enhanced MR imaging	0.580	0.762	0.627
Dynamic 3D-VIBE MR imaging	0.578	0.701	0.610

Data are *k* values indicating the agreement between pairs of observers regarding the presence or absence of HCC.

(Fig. 2). Retrospective analysis by all observers of the missed lesions on ferumoxides-enhanced MR imaging showed that three of the four missed lesions were isointense relative to the surrounding liver parenchyma and was confirmed as well-differentiated HCC at surgery or on percutaneous biopsy; the other lesion was misdiagnosed as a heterogeneous fibrotic area (Fig. 1). HCCs missed on the gadolinium-enhanced dynamic 3D-VIBE MR imaging were detected by the three observers on ferumoxides-enhanced MR imaging as follows: observer 1, one tumor in one patient; observer 2, six tumors in six patients; observer 3, four tumors in four patients. One tumor missed by all observers on gadolinium-enhanced dynamic 3D-VIBE MR imaging was detected on ferumoxides-enhanced MR imaging. This lesion showed isosignal intensity to the surrounding liver parenchyma, but was confirmed as HCC on percutaneous biopsy. In addition, tumors not detected by the two imaging modalities were as follows according to the three observers: observer 1, four tumors in four patients; observer 2, one tumor in one patient; observer 3, two tumors in two patients. For one tumor, no observer could detect the lesion on either MR examination. This lesion could not be seen on retrospective reviewing, but was demonstrated to be 5 mm in diameter on intraoperative sonography and was confirmed as HCC on surgical resection.

#### Positive predictive values

The number of true-positive observations at confidence levels of 3 or 4, the number of false-positives and the false-positive rate (false-positive/true-positives) between the two imaging modalities are shown in Table 4. On ferumoxides-enhanced MR imaging, the observers detected 25 false-positive lesions. Of these false-positive lesions, 20 (80%) were attributed to the vessels and the remainder (20%) were due to inhomogeneous signal decrease in cirrhosis-related fibrotic area (Fig. 3). On gadolinium-enhanced dynamic 3D-VIBE MR imaging, the observers detected 23 false-positive lesions. Of these lesions, 21 (91.3%) were attributed to misdiagnosis of the shunts as tumor nodules, and the remaining two lesions were due to either heterogeneous enhancement or to actually being a dysplastic nodule.

#### Interobserver agreement

For two imaging modalities, kappa values for the three observers were between 0.578 and 0.762, respectively, thereby indicating good interobserver agreement (Table 5).

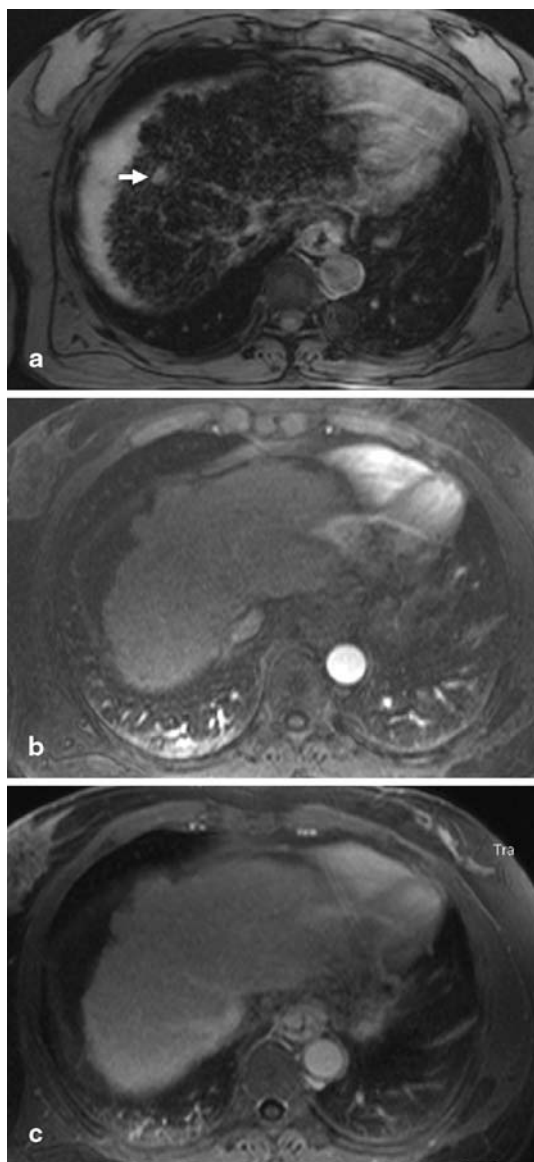


**Fig. 3** A 63-year-old man with severe liver cirrhosis and hepatocellular carcinoma in segment 5 of the liver (not shown). **a** Ferumoxides-enhanced breath-hold T2\*-weighted fat image obtained with steady-state procession shows a discrete round high-signal-intensity lesion (*arrow*). All observers interpreted this lesion to be a small hepatocellular carcinoma. **b, c** Small lesion corresponding to hepatocellular carcinoma seen on **a** is not shown on the gadolinium-enhanced 3D-VIBE image obtained during **b** the arterial phase and **c** equilibrium phase. There was no evidence of the presence of hepatic lesions in that area on the 6-month follow-up images (not shown). The false-positive lesions on MR imaging were attributed to reticular fibrosis due to severe cirrhotic parenchyma. All observers interpreted this lesion as a small hepatocellular carcinoma

## Discussion

Several studies have been reported regarding the efficacy of ferumoxides-enhanced hepatic MR imaging for the detection of focal liver lesions, including HCC and hepatic metastases [1–8]. Yamamoto et al. [19] reported the improved detectability of small HCC lesions after enhancement with ferumoxides. In addition, Choi et al. [6] reported that ferumoxides-enhanced MR imaging had the potential to replace CT during both arterial portography and hepatic arteriography, and is the best imaging modality for the detection of HCC. However, there are some possible limitations to using ferumoxides-enhanced MR imaging for the detection of HCC in patients with liver cirrhosis [20–22]. One major limitation is related to the signal decrease of the liver parenchyma after ferumoxides administration possibly being less in chronically injured liver tissue than in healthy liver tissue because of the decreased functioning of the Kupffer cells [23]. Given that most HCCs occur in chronically injured liver tissue and the effect of decreasing signal intensity of the ferumoxides particles taken up by the Kupffer cells could be suboptimal in cirrhotic liver, the increasing effect of lesion-to-liver CNR by ferumoxides particles on T2-weighted images, could be suboptimal. Furthermore, there is only limited use of ferumoxides-enhanced MR imaging for lesion characterization because of the impracticality of dynamic phase imaging.

There is a clinical need to determine the optimal contrast material for liver MR imaging in order to detect hypervascular HCC. Despite several reports regarding this issue, it is controversial whether ferumoxides-enhanced or gadolinium-enhanced MR imaging is optimal for the detection of HCC in patients with liver cirrhosis. Vogl et al. [24] detected more HCC nodules with ferumoxides-enhanced MR imaging than with dynamic gadolinium-enhanced MR imaging. In contrast, Tang et al. [20] reported gadolinium-enhanced MR imaging to be more variable than ferumoxides-enhanced MR imaging for the detection of HCCs. In addition, Pauleit et al. [25] detected more small HCC nodules (<1.5 cm) with dynamic gadolinium-enhanced MR imaging than with ferumoxides-enhanced MR imaging. Furthermore, several authors have reported that by using combined contrast MR methods, i.e., combined gadolinium-enhanced and ferumoxides-enhanced MR imaging, compared with single contrast-enhanced imaging, the diagnosis of HCC could be improved [26–28].

For the detection of HCCs on gadolinium-enhanced MR imaging, it is crucial to acquire good quality arterial-phase imaging in terms of temporal and spatial resolution because of the increased arterial blood supply of an HCC compared to that of liver parenchyma. Given that gadolinium-based contrasts are diffused into the extracellular space within a few minutes after the intravenous injection, the use of imaging techniques with high tem-

poral resolution is warranted. Based on recent studies regarding 3D-GRE techniques [10, 11], 3D-GRE techniques have been proven to have several advantages over 2D-GRE techniques. For example, contiguous and thinner slice images can be obtained during the breath-hold, thereby decreasing problems with the partial volume effect [10, 11]. In this study, we used a modified 3D-GRE sequence, VIBE, for dynamic MR imaging as it is optimized for short acquisition times and achieves high-spatial-resolution imaging with excellent anatomic detail through the use of asymmetric *k*-space sampling and interpolation [13].

Our study results demonstrate that in AFROC analysis, all three observers achieved higher diagnostic performance with gadolinium-enhanced 3D VIBE dynamic MR imaging than with ferumoxides-enhanced MR imaging (mean Az on gadolinium-enhanced dynamic 3D-VIBE MR imaging, 0.95; mean Az on ferumoxides-enhanced MR imaging, 0.90;  $P=0.057$ ). In addition, in terms of mean sensitivity, gadolinium-enhanced dynamic 3D-VIBE MR imaging performed better than ferumoxides-enhanced MR imaging (90.7 vs. 80.9%;  $P=0.03$ ). In this respect, our results agreed with those of Tang et al. [20]. Furthermore, the mean sensitivity of the gadolinium-enhanced dynamic 3D-VIBE MR images (85.2%) was significantly higher than that of the ferumoxides-enhanced MR images (69.4%) in lesions smaller than 15 mm in diameter ( $P<0.05$ ).

The following factors may have contributed to our results of substantially superior accuracy and sensitivity with gadolinium-enhanced dynamic 3D-VIBE MR imaging of HCCs. First, we obtained the gadolinium-enhanced dynamic MR imaging using a modified 3D-gradient technique, i.e., VIBE [13]. Given that VIBE achieves high temporal and spatial resolution imaging through the use of asymmetric *k*-space sampling and interpolation and permits thinner images (2.5 mm slice thickness) than the 2D-gradient technique, this VIBE technique is more suitable for the detection of small lesions than T2-weighted or T2\*-weighted images, which have thicker slices. Secondly, after intravenous administration of ferumoxides particles, reticular fibrosis of cirrhotic liver parenchyma shows high-signal intensity,

which can obscure small HCCs [20]. Third, in our study there were nine patients with severe cirrhosis (Child score C). Since severely cirrhotic livers show poor liver enhancement because of the decreased activity of Kupffer's cells to phagocytes ferumoxides particles [29, 30], the effect of SPIO to increase lesion-to-liver CNR may not be strong in this clinical scenario.

Our study has some limitations. First, not all lesions were histologically confirmed. However, surgical proof of the presence of HCC is becoming difficult to obtain because in many circumstances small HCCs are treated using interventional procedures such as TACE and/or percutaneous radiofrequency ablation because of the limited hepatic functional reserve. However, all of the lesions we detected were subjected to several confirming studies, such as CT hepatic arteriography, CT during arterial portography or CT after arterial infusion of iodized oil [31, 32] and at least 6-month follow-up studies, all of which should support the present study results. Second, we did not include T1-weighted images when we evaluated the diagnostic accuracy of ferumoxides-enhanced MR images because T2-weighted and T2\*-weighted images have been regarded as the two best sequences for revealing SPIO-induced signal decrease [15, 16]. However, considering that ferumoxides-enhanced T1-weighted images could be helpful to avoid false positive diagnosis, interpretation of ferumoxides-enhanced T2-weighted and T2\*-weighted images may result in underestimation of diagnostic accuracy of ferumoxides-enhanced MRI for detection of HCC.

In conclusion, our study results confirm that the mean sensitivity of the gadolinium-enhanced dynamic 3D-VIBE MR imaging was superior to that of our ferumoxides-enhanced MR imaging. In addition, there was a trend toward better diagnostic accuracy for dynamic MR imaging than ferumoxides-enhanced MR imaging. Therefore, we suggest that gadolinium-enhanced MR imaging using a 3D-VIBE sequence should be preferable to ferumoxides-enhanced MR imaging for the detection of HCC.

**Acknowledgment** The authors thank Bonnie Hami, M.A., Department of Radiology, University Hospitals of Cleveland (Ohio), for her editorial assistance in the preparation of this manuscript.

## References

1. Ward J, Naik KS, Guthrie JA, Wilson D, Robinson PJ (1999) Hepatic lesion detection: comparison of MR imaging after the administration of superparamagnetic iron oxide with dual-phase CT by using alternative-free response receiver operating characteristic analysis. *Radiology* 210:459–466
2. Vogl TJ, Schwarz W, Blume S, Pietsch M, Shamsi K, Franz M, Lobeck H, Balzer T, del Tredici K, Neuhaus P, Felix R, Hammerstingl RM (2003) Preoperative evaluation of malignant liver tumors: comparison of unenhanced and SPIO (Resovist)-enhanced MR imaging with biphasic CTAP and intraoperative US. *Eur Radiol* 13:262–272
3. Ros PR, Freeny PC, Harms SE, Seltzer SE, Davis PL, Chan TW, Stillman AE, Muroff LR, Runge VM, Nissenbaum MA (1995) Hepatic MR imaging with ferumoxides: a multicenter clinical trial of the safety and efficacy in the detection of focal hepatic lesions. *Radiology* 196:481–488

4. Kim SK, Kim SH, Lee WJ, Kim H, Seo JW, Choi D, Lim HK, Lee SJ, Lim JH (2002) Preoperative detection of hepatocellular carcinoma: ferumoxides-enhanced versus mangafodipir trisodium-enhanced MR imaging. *Am J Roentgenol* 179:741–750
5. Kang BK, Lim JH, Kim SH, Choi D, Lim HK, Lee WH, Lee SJ (2003) Preoperative depiction of hepatocellular carcinoma: ferumoxides-enhanced MR imaging versus triple-phase helical CT. *Radiology* 226:79–85
6. Choi D, Kim SH, Lim JH, Lee WJ, Jang HJ, Lee SJ (2001) Preoperative detection of hepatocellular carcinoma: ferumoxides-enhanced MR imaging versus combined CT during arterial portography and CT hepatic arteriography. *Am J Roentgenol* 176:475–482
7. Matsuo M, Kanematsu M, Itoh K, Ito K, Maetani Y, Kondo H, Kako N, Matsunaga N, Hoshi H, Shiraishi J (2001) Detection of malignant hepatic tumors: comparison of gadolinium- and ferumoxides-enhanced MR imaging. *Am J Roentgenol* 177:637–643
8. Del Frate CD, Bazzocchi M, Mortele KJ, Zuiani C, Londero V, Como G, Zanardi R, Ros PR (2002) Detection of liver metastases: comparison of gadobenate dimeglumine-enhanced and ferumoxides-enhanced MR imaging examinations. *Radiology* 225:766–772
9. Stark DD, Weissleder R, Elizondo G, Hahn PF, Saini S, Todd LE, Wittenberg J, Ferrucci JT (1988) Superparamagnetic iron oxide: clinical application as a contrast agent for MR imaging of the liver. *Radiology* 168:297–301
10. Siegelman ES, Outwater EK (1998) MR imaging techniques of the liver. *Radiol Clin North Am* 36:263–286
11. Kim YK, Lee JM, Kim CS (2004) Gadobenate dimeglumine-enhanced liver MR imaging: value of dynamic and delayed imaging for the characterization and detection of focal liver lesions. *Eur Radiol* 14:5–13
12. Yoshimitsu K, Honda H, Jimi M, Kuroiwa T, Irie H, Aibe H, Shinozaki K, Asayama Y, Shimada M, Masuda K (2001) Correlation of three-dimensional gradient echo dynamic MR imaging with CT during hepatic arteriography in patients with hypervascular hepatocellular carcinomas: preliminary clinical experience. *J Magn Reson Imaging* 13:258–262
13. Rofsky NM, Lee VS, Laub G, Pollack MA, Krinsky GA, Thomasson D, Ambrosino M, Weinreb JC (1999) Abdominal MR imaging with a volumetric interpolated breath-hold examination. *Radiology* 212:876–884
14. Pugh RN, Murray-Lyon IM, Dawson JL, Pietroni MC, Williams R (1973) Transection of the esophagus for bleeding esophageal varices. *Br J Surg* 60:636–649
15. Kim SH, Choi DI, Lim JH (2002) Optimal pulse sequence for ferumoxides-enhanced MR imaging used in the detection of hepatocellular carcinoma: a comparative study using seven pulse sequences. *Korean J Radiol* 3:87–97
16. Fretz CJ, Elizondo G, Weissleder R, Hahn PF, Stark DD, Ferrucci JT (1989) Superparamagnetic iron oxide-enhanced MR imaging: pulse sequence of optimization for detection of liver cancer. *Radiology* 172:393–397
17. Hussain HK, Londy FJ, Francis IR, Nghiem HV, Weadock WJ, Gebremariam A, Chenevert TL (2003) Hepatic arterial phase MR imaging with automated bolus-detection three-dimensional fast gradient-recalled-echo sequence: comparison with test-bolus method. *Radiology* 226:558–566
18. Chakraborty DP, Winter LH (1990) Free-response methodology: alternate analysis and a new observer-performance experiment. *Radiology* 174:873–881
19. Yamamoto H, Yamachita Y, Yoshimatsu S, Baba Y, Hatanaka Y, Murakami R, Nishiharu T, Takahashi M, Higashida Y, Moribe N (1995) Hepatocellular carcinoma in cirrhotic liver: detection with unenhanced and iron-oxide-enhanced MR imaging. *Radiology* 195:106–112
20. Tang Y, Yamashita Y, Arakawa A, Namimoto T, Mitsuzaki K, Abe Y, Katahira K, Takahashi M (1999) Detection of hepatocellular carcinoma arising in cirrhotic livers: comparison of gadolinium- and ferumoxine-enhanced MR imaging. *Am J Roentgenol* 172:1547–1554
21. Elizondo G, Weissleder R, Stark DD, Guerra J, Garza J, Fretz CJ, Todd LE, Ferrucci JT (1990) Hepatic cirrhosis and hepatitis: MR imaging enhanced with superparamagnetic iron oxide. *Radiology* 174:797–801
22. Denys A, Arrive L, Servois V, Dubray B, Najmark D, Sibert A, Menu Y (1994) Hepatic tumors: detection and characterization at 1 T MR imaging enhanced with AMI-25. *Radiology* 193:665–669
23. Yamashita Y, Mitsuzaki K, Yi T, Ogata I, Nishiharu T, Urata J, Takahashi M (1996) Small hepatocellular carcinoma in patients with chronic liver damage: prospective comparison of detection with dynamic MR imaging and helical CT of the whole liver. *Radiology* 200:79–84
24. Vogl TJ, Hammerstingl R, Schwarz W, Mack MG, Muller PK, Pegios W, Keck H, Eibl-Eibesfeldt A, Hoelzl J, Woessner B, Bergman C, Felix R (1996) Superparamagnetic iron oxide-enhanced versus gadolinium-enhanced MR imaging for differential diagnosis of focal liver lesions. *Radiology* 198:881–887
25. Pauleit D, Textor J, Bachmann R, Conrad R, Flacke S, Layer G, Kreft B, Schild H (2002) Hepatocellular carcinoma: detection with gadolinium- and ferumoxides-enhanced MR imaging of the liver. *Radiology* 222:73–80
26. Ward J, Guthrie J, Scott DJ, Atchley J, Wilson D, Davies MH, Wyatt JI, Robinson PJ (2000) Hepatocellular carcinoma in the cirrhotic liver: double-contrast MR imaging for diagnosis. *Radiology* 216:154–162
27. Kondo H, Kanematsu M, Hoshi H, Murakami T, Kim T, Hori M, Matsuo M, Nakamura H (2000) Preoperative detection of malignant hepatic tumors: comparison of combined methods of MR imaging with combined methods of CT. *Am J Roentgenol* 174:947–954
28. Kwak HS, Lee JM, Kim CS (2004) Preoperative detection of hepatocellular carcinoma: comparison of combined contrast-enhanced MR imaging and combined CT during arterial portography and CT hepatic arteriography. *Eur Radiol* 14:447–457
29. Clement O, Frija G, Chambon C, Schouman-Claes E, Mosnier JF, Poupon MF, Balkau B (1991) Liver tumors in cirrhosis: experimental study with ferumoxides-enhanced MR imaging. *Radiology* 180:31–36
30. Imai Y, Murakami T, Yoshida S, Nishikawa M, Ohsawa M, Tokunaga K, Murata M, Shibata K, Zushi S, Kurokawa M, Yonezawa T, Kawata S, Takamura M, Nagano H, Sakon M, Monden M, Wakasa K, Nakamura H (2000) Superparamagnetic iron oxide-enhanced magnetic resonance images of hepatocellular carcinoma: correlation with histological grading. *Hepatology* 32:205–212
31. Ohishi H, Uchida H, Yoshimura H, Ohue S, Ueda J, Katsuragi M, Matsuo N, Hosogi Y (1985) Hepatocellular carcinoma detected by iodized oil: use of anticancer agents. *Radiology* 154:25–29
32. Yumoto Y, Jinno K, Tokuyama K, Araki Y, Ishimitsu T, Maeda H, Konno T, Iwamoto S, Ohnishi K, Okuda K (1985) Hepatocellular carcinoma detected by iodized oil. *Radiology* 154:19–24